INTERNATIONAL JOURNAL FOR NUMERICAL METHODS IN FLUIDS
Int. J. Numer. Meth. Fluids 2001; **37**: 341–359 (DOI: 10.1002/fld.177)

The discontinuous profile method for simulating two-phase flow in pipes using the single component approximation

Vincent Guinot*,[1]

International Institute for Infrastructure Hydraulic and Environmental Engineering—IHE, Delft, Netherlands

SUMMARY

Godunov-type algorithms are very attractive for the numerical solution of discontinuous flows. The reconstruction of the profile inside the cells is crucial to scheme performance. The non-linear generalization of the discontinuous profile method (DPM) presented here for the modelling of two-phase flow in pipes uses a discontinuous reconstruction in order to capture shocks more efficiently than schemes using continuous functions. The reconstructed profile is used to define the Riemann problem at cell interfaces by averaging of the components of the variable in the base of eigenvectors over their domain of dependence. Intercell fluxes are computed by solving the Riemann problem with an approximate-state solver. The adapted treatment of boundary conditions is essential to ensure the quality of the computational results and a specific procedure using virtual cells at both extremities of the computational domain is required. Internal boundary conditions can be treated in the same way as external ones. Application of the DPM to test cases is shown to improve the quality of computational results significantly. Copyright © 2001 John Wiley & Sons, Ltd.

KEY WORDS: boundary conditions; Godunov schemes; reconstruction; Riemann solvers; two-phase flow

1. INTRODUCTION

The modelling of two-phase flow in pipe systems has a wide range of possible applications to industrial design, amongst which may be mentioned the design of hydraulic and nuclear power plants. Apart from difficulties arising from the interaction between the fluid and the mechanical structure, the computation of such flow poses two problems. The first one is the influence of highly variable wave speeds on the behaviour of the solution and the handling of strong shock waves. The second one is related to the high number of reflections to which the waves are subject and the subsequent effort that must be devoted to the treatment of boundary

* Correspondence to: International Institute for Infrastructure Hydraulic and Environmental Engineering—IHE, Westvest 7, PO Box 3015, 2601 DA Delft, Netherlands.
[1] E-mail: vgt@ihe.nl

Received November 1999
Revised December 2000

conditions. The first problem has been abundantly addressed in the past in the field of gas dynamics and free-surface flow, but the latter is more specific to network problems and the implications of the use of high-order schemes in algorithms for hydraulic networks have not yet been much explored. The aim of this paper is to provide solutions for the one-dimensional modelling of two-phase flows in pipe networks under the single component approximation using a higher-order Godunov-type scheme.

Under the assumption of a small fraction of gas, the equations describing two-phase flows in pipes of a can be written in the following conservative form:

$$\frac{\partial \phi}{\partial t} + \frac{\partial F}{\partial x} = 0 \tag{1.1a}$$

$$\phi = \begin{bmatrix} \mu \\ q \end{bmatrix}, \qquad F = \begin{bmatrix} q \\ Ap + q^2/\mu \end{bmatrix} \tag{1.1b}$$

$$\frac{\mathrm{d}}{\mathrm{d}\mu}(Ap) = c^2 = \frac{c_w^2}{1 + \theta/p^{1+1/\alpha}} \tag{1.1c}$$

$$\theta = \eta_0 \rho_0 c_w^2 p_0^{1/\alpha} \tag{1.1d}$$

$$p\eta^{\alpha} = p_0 \eta_0^{\alpha} \tag{1.1e}$$

$$\rho_g \eta = \rho_{g,0} \eta_0 \tag{1.1f}$$

where A (m^2) is the pipe cross-sectional area, c ($\mathrm{m\ s}^{-1}$) is the local speed of sound in the mixture, c_w ($\mathrm{m\ s}^{-1}$) is the local speed of sound in the absence of gas, p (Pa) is the pressure, p_0 (Pa) is a reference pressure, q ($\mathrm{kg\ s}^{-1}$) is the mass discharge, α (dimensionless) is a coefficient characterizing the behaviour of the gas fraction, η (dimensionless) is the fraction of volume occupied by the gas phase, η_0 (dimensionless) is the value of η for the reference pressure p_0, μ ($\mathrm{kg\ m}^{-1}$) is the mass per unit length of pipe, ρ_g ($\mathrm{kg\ m}^{-3}$) is the fluid density and $\rho_{g,0}$ ($\mathrm{kg\ m}^{-3}$) is the fluid density at pressure p_0. Equations (1.1c) and (1.1d) for the celerity are a generalization [4] of a formula provided by other authors [1,2] under the assumption of no slip between the gas and the liquid phases. Equation (1.1e) is obtained from the assumption that there is no exchange of mass between the two phases, which is confirmed by experimental studies [3] that showed that the transients are too fast for such exchanges to take place. Therefore, it is possible to deal with the two phases simultaneously as if they formed a single fluid (hence the name of 'single component approximation'). Note that the single component approximation can be used reliably only for small void ratios. The local sound speed—and therefore the wave celerity—is extremely sensitive to the value of the pressure and may easily vary by a factor of 10^2 or 10^3 along the pipe. Shocks are then likely to appear and numerical methods that can handle them are needed. Godunov-type algorithms then appear as very good candidates, for they can handle any type of wave via the solution of Riemann problems at the interfaces between the computational cells. A first step in the present work [4] consisted of

studying the feasibility of the solution of the equations above by the first-order, original Godunov scheme. The conclusions of this work were, among others, that although robust and reliable, the first-order Godunov scheme was not accurate enough and that higher-order schemes were needed. However, the implementation of such schemes is not straightforward, for the following reason.

A feature of pipe transients is that, due to network complexity and to the contrast in the length of the pipes, the pressure waves may cover several times the pipe length before the pressure (or depression) peak is reached. The waves are reflected many times at the pipes boundaries and the accurate computation of their reflections is essential to the quality of the numerical solution. In particular, the author showed in a previous publication [5] that all the benefits brought by high-order schemes to compute the waves inside the pipe may be lost if the problem of boundary conditions is neglected. This is also confirmed by a number of unpublished numerical experiments carried out in the framework of the present study, where it was seen that a poor treatment of boundary conditions may lead to more degraded solutions when combined with higher-order schemes than with the first-order Godunov method. In addition to the classical problem of sharp fronts and shock modelling, a careful treatment of boundary conditions was therefore devised.

Section 2 presents the solution technique used, from the reconstruction step to the computation of intercell fluxes. The treatment of boundary conditions is detailed in Section 3. A computational example is provided in Section 4. Concluding remarks are eventually provided in Section 5.

2. TREATMENT OF INTERNAL CELLS

2.1. Outline of the Godunov technique

The Godunov technique is a finite volume-based algorithm that is based on the weak solution of the flow Equations (1.1). After discretization of space into a set of computational cells, Equation (1.1a) becomes

$$\Phi_i^{n+1} = \Phi_i^n + \frac{\Delta t}{\Delta x_i}\left(F_{i-1/2}^{n+1/2} - F_{i+1/2}^{n+1/2}\right) \tag{2.1}$$

where Φ_i^n is the average value of ϕ over cell i, and $F_{i-1/2}^{n+1/2}$ is the average value of the flux F at the interface between cells *i-1* and *i* over the time interval $\Delta t = t^{n+1} - t^n$. The value of the flux at each interface is determined by the initial distribution of the variable on both sides of this interface. To compute the fluxes, a three-step algorithm is used, to be detailed in the sequel.

Firstly, the initial distribution of the variable inside a given cell i is determined from the average values Φ_i in this cell and the neighbouring ones. This is called the reconstruction step.

The reconstructed profile is then used to define a Riemann problem at each interface $i+1/2$ between cells i and $i+1$, i.e. an initial value problem of the form

$$\phi(x) = \phi_{i+1/2,\mathrm{L}} \quad \text{for } x \le x_{i+1/2} \tag{2.2a}$$

$$\phi(x) = \phi_{i+1/2,\mathrm{R}} \quad \text{for } x > x_{i+1/2} \tag{2.2b}$$

where $x_{i+1/2}$ is the abscissa of the interface and $\phi_{i+1/2,\mathrm{L}}$ and $\phi_{i+1/2,\mathrm{R}}$ are called the left and right states respectively. These left and right states depend directly on the reconstructed profile of the previous step.

The Riemann problem is then solved to provide the value $\phi_{i+1/2}$ of ϕ at the interface. The flux $F_{i+1/2}$ is computed using

$$F_{i+1/2} = F(\phi_{i+1/2}) \tag{2.3}$$

2.2. The DPM reconstruction

The reconstruction step is a crucial point in the performance of the numerical scheme. The scheme designed by Godunov in 1959 [6] was based on a constant profile. Later on, many authors presented various options for the reconstruction [7–9]. In all these approaches, the reconstructed profiles are discontinuous at the cell interfaces only. This hypothesis does not allow the location of discontinuities that are inside the computational cells. The approach chosen for the present scheme consists of using a discontinuous reconstruction inside the computational cells, hence the name of the scheme (discontinuous profile method, or DPM). Here the non-linear generalization of this approach is presented.

Consider one-dimensional advection of a variable ϕ, and assume that space is discretized into computational cells of length Δx_i. At a given time, the average values Φ_i of ϕ over the cells are assumed to be known. The profile is reconstructed over cell i as follows (see Figure 1)

$$\phi(x) = \phi_{i,\mathrm{L}} \quad \text{for } x \leq \alpha_i \Delta x_i \tag{2.4a}$$

$$\phi(x) = \phi_{i,\mathrm{R}} \quad \text{for } x > \alpha_i \Delta x_i \tag{2.4b}$$

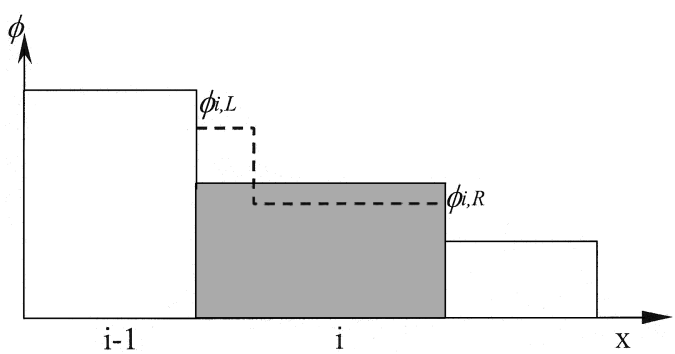

Figure 1. Discontinuous reconstruction of the profile over a computational cell. The solid line represents the average value over the cell; the dashed line shows the reconstructed profile.

$$\alpha_i \in [0, 1] \tag{2.4c}$$

Note that $\phi_{i,\mathrm{L}}$ and $\phi_{i,\mathrm{R}}$ should not be confused with the left and right states $\phi_{i+1/2,\mathrm{L}}$ and $\phi_{i+1/2,\mathrm{R}}$ of the Riemann problem, which are related to the left and right sides of the cell edge. To satisfy mass conservation, $\alpha_{i,\mathrm{L}}$ must satisfy

$$\alpha_i \phi_{i,\mathrm{L}} + (1 - \alpha_i)\phi_{i,\mathrm{R}} = \Phi_i \tag{2.5}$$

which gives

$$\alpha_i = \frac{\Phi_i - \phi_{i,\mathrm{R}}}{\phi_{i,\mathrm{L}} - \phi_{i,\mathrm{R}}} \tag{2.6}$$

Therefore, α_i is uniquely determined from the left and right states $\phi_{i,S}$, $S = \mathrm{L}, \mathrm{R}$. These are computed using a linear interpolation between the averages over the cells

$$\phi_{i,\mathrm{L}} = \beta_{i,\mathrm{L}} \Phi_{i-1} + (1 - \beta_{i,\mathrm{L}})\Phi_i \tag{2.7a}$$

$$\phi_{i,\mathrm{R}} = \beta_{i,\mathrm{R}} \Phi_{i+1} + (1 - \beta_{i,\mathrm{R}})\Phi_i \tag{2.7b}$$

$$\beta_{i,S} \in [0, 1], \quad S = \mathrm{L},\ \mathrm{R} \tag{2.7c}$$

Equation (2.7c) is a necessary condition for the monotonicity of the solution [7]. The value of $\beta_{i,S}$, $S = \mathrm{L}, \mathrm{R}$, depends on the local features of the profile and in particular on its monotonicity. The monotonicity indicator ω is defined as follows:

$$\omega_i = s_{i-1/2} s_{i+1/2} \tag{2.8a}$$

$$s_{i-1/2} = 2 \frac{\Phi_i - \Phi_{i-1}}{\Delta x_{i-1} + \Delta x_i} \tag{2.8b}$$

$\omega_i < 0$ means that Φ_i is a local extremum, $\omega_i = 0$ indicates that Φ_i has the same value as one of its neighbouring cells, and $\omega_i > 0$ is found in the case of a monotonic profile. In the case $\omega_i < 0$, the only way to satisfy Equation (2.5) is to set both $\beta_{i,\mathrm{L}}$ and $\beta_{i,\mathrm{R}}$ to zero. In other cases, $\beta_{i,S}$ must be given a value such that the reconstructed profile is as smooth as possible, otherwise leading to artificial steepening of the profile and to the formation of discontinuities that are not justified physically. Consider a profile with a constant slope over cell i, i.e. obeying the law

$$\varphi_i(x) = \Phi_i + s_i x \tag{2.9}$$

where the origin of x is located at the centre of cell i. In order to emulate second-order accuracy, a reconstruction $\phi_i(x)$ is looked for that is a close as possible to this 'target' profile.

Due to symmetry considerations, we set $\beta_{i,\mathrm{L}} = \beta_{i,\mathrm{R}} = \beta$. To do so, the two functions f and g are defined as the primitive functions of φ_i and ϕ_i respectively

$$f(x) = \int_{-\Delta x_i/2}^{x} \varphi_i(x)\,\mathrm{d}x \tag{2.10a}$$

$$g(x) = \int_{-\Delta x_i/2}^{x} \phi_i(x)\,\mathrm{d}x \tag{2.10b}$$

the analytical expression for $f(x)$ is obtained by integrating Equation (2.9)

$$f(x) = (x + \Delta x_i/2)\Phi_i + (x^2 - \Delta x_i^2/4)s_i/2 \tag{2.11}$$

The expression for $g(x)$ is deduced from Equations (2.4a) and (2.4b)

$$g(x) = \{\min[x, (\alpha_i - 1/2)\Delta x_i] + \Delta x_i/2\}\,\phi_{i,\mathrm{L}} + \{\max[x, (\alpha_i - 1/2)\Delta x_i] - (\alpha_i - 1/2)\Delta x_i\}\,\phi_{i,\mathrm{R}} \tag{2.12}$$

Figure 2 shows the shapes of f and g. f is a parabolic function, the second-order derivative of which has the same sign as the slope s_i. g is a piecewise linear function, the slope of which is equal to either $\phi_{i,\mathrm{L}}$ or $\phi_{i,\mathrm{R}}$ depending on the value of x. The primitive function for the original, constant Godunov reconstruction, also shown on the figure, is a straight line. From Equations (2.7a) and (2.7b) we obtain

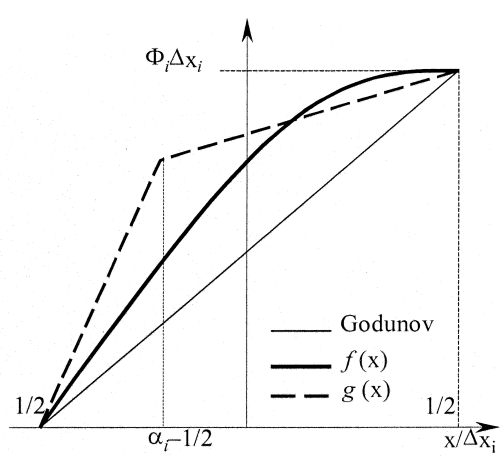

Figure 2. Shapes of f and g.

$$\phi_{i,\mathrm{L}} = \Phi_i - \beta s_i \Delta x_i \tag{2.13a}$$

$$\phi_{i,\mathrm{R}} = \Phi_i + \beta s_i \Delta x_i \tag{2.13b}$$

In particular, the discontinuity between $\phi_{i,\mathrm{L}}$ and $\phi_{i,\mathrm{R}}$ should not be too important, otherwise leading to an artificial steepening of the profile. Therefore $g(x)$ should be equal to $f(x)$ at the discontinuity between $\phi_{i,\mathrm{L}}$ and $\phi_{i,\mathrm{R}}$, i.e. for $x = (\alpha_i - 1/2)\Delta x_i$. Substituting this condition into Equations (2.11) and (2.12) yields

$$\Phi_i \Delta x_i \alpha_i + (\alpha_i^2 - \alpha_i)\Delta x_i^2 s_i/2 = (\Phi_i - \beta s_i \Delta x_i)\alpha_i \Delta x_i \tag{2.14}$$

which simplifies into

$$\beta = (1 - \alpha_i)/2 \tag{2.15}$$

As α_i is dependent on β (via Equations (2.6) and (2.7)), Equation (2.15) cannot be satisfied in all cases. The best compromise is to satisfy this equality in average, i.e. for $\alpha_i = \frac{1}{2}$. This gives

$$\beta = 1/4 \tag{2.16}$$

Note that any higher value of β leads to profile steepening and that a lower value introduces smearing. The constant reconstruction of the original Godunov scheme can be seen as a particular case of the present one, with $\beta = 0$. As such, this reconstruction does bring some improvements as compared with the first-order scheme, but is not sufficient to guarantee the preservation of steep fronts and strong shocks. Therefore, an additional modification is introduced that consists of setting the coefficient $\beta_{i,S}$ to 1 if the cell located on side S of cell i is a local extremum. This can be formulated as

$$\text{if } \beta_{i,\mathrm{L}} = 1 \text{ if } \omega_{i-1} \leq 0,\ \beta_{i,\mathrm{L}} = 1/4 \text{ otherwise} \tag{2.17a}$$

$$\text{if } \beta_{i,\mathrm{R}} = 1 \text{ if } \omega_{i+1} \leq 0,\ \beta_{i,\mathrm{R}} = 1/4 \text{ otherwise} \tag{2.17b}$$

2.3. Characterization of the Riemann problem

At the interface between two computational cells, the reconstructed profile is used to define the Riemann problem by averaging the eigenvectors over their domain of dependence. In the case of subcritical flow—as it is the case in most pipe transient simulations—this is equivalent to averaging the variable ϕ itself over the domain of dependence of the invariants. In the case of supercritical flow, the procedure is more complicated, as detailed below.

The flux at the interface is given by

$$F_{i+1/2} = F(\phi_{i+1/2}) = F(\mathbf{K}\sigma_{i+1/2}) \tag{2.18a}$$

$$\mathbf{K} = \begin{bmatrix} 1 & 1 \\ \lambda_1 & \lambda_2 \end{bmatrix} \tag{2.18b}$$

$$\lambda_k = q/\mu + (-1)^k c \tag{2.18c}$$

where $\mathbf{K}$ is the matrix formed by the eigenvectors of the Jacobian matrix $\mathbf{M} = \partial F/\partial \phi$ (see Appendix A for details on the derivation of $\mathbf{M}$), λ_k, $k = 1, 2$ are the eigenvalues of $\mathbf{M}$, and $\sigma = \mathbf{K}^{-1}\phi$ contains the co-ordinates of ϕ in the base of the eigenvectors. The derivation of $\mathbf{K}$ is given in Appendix A. In the case of a Riemann problem, i.e. with constant right and left states, $\sigma_{i+1/2}$ is a constant. The DPM reconstruction defines a generalized Riemann problem, where both states are not necessarily constant. In that case, the value of $\sigma_{i+1/2}$ depends on time. We are therefore interested in the average $\bar{F}_{i+1/2}$ of the flux $F_{i+1/2}$ over time

$$\bar{F}_{i+1/2} = \frac{1}{\Delta t}\int_0^{\Delta t} F_{i+1/2}(t)\,\mathrm{d}t \tag{2.19}$$

To estimate this value, a linearization is applied to approximate $\bar{F}_{i+1/2}$ with

$$\bar{F}_{i+1/2} = F(\mathbf{K}\bar{\sigma}_{i+1/2}) \tag{2.20a}$$

$$\bar{\sigma}_{i+1/2} = \frac{1}{\Delta t}\int_0^{\Delta t} \sigma_{i+1/2}(t)\,\mathrm{d}t \tag{2.20b}$$

By performing a variable change along the k-th characteristic curve, the kth component $\bar{\sigma}^{(k)}_{i+1/2}$ of $\bar{\sigma}_{i+1/2}$ is given by

$$\bar{\sigma}^{(k)}_{i+1/2} = \frac{1}{\Delta t}\int_0^{\Delta t} \sigma^{(k)}_{i+1/2}(t)\,\mathrm{d}t = \frac{1}{\zeta_k}\int_{x_{i+1/2}-\zeta_k}^{x_{i+1/2}} \sigma^{(k)}_j(x)\,\mathrm{d}x \tag{2.21}$$

where $\zeta_k = \lambda_k \Delta t$ is the horizontal distance covered by the kth characteristic during time Δt (also called the domain of dependence associated to the kth characteristic). Index j denotes the cell in which the foot of the characteristic is located.

Assume that $j = i$. If both λ_1 and λ_2 are positive in cell i (supercritical flow), then both components of $\bar{\sigma}_i$ are fully determined in cell i, because both domains of dependence of the interface $i + \frac{1}{2}$ lie in cell i. The left state $\phi_{i+1/2,\mathrm{L}}$ is then deduced from

$$\phi_{i+1/2,\mathrm{L}} = \mathbf{K}\bar{\sigma}_i \tag{2.22}$$

Pipe transients are characterized by subcritical flows. In that case the foot of the second characteristic only lies in cell i, whereas the first one has its foot in cell $i+1$. Consequently, the value of the first component $\bar{\sigma}^{(1)}_i$ of $\bar{\sigma}_i$ does not have any influence on the solution of the Riemann problem at interface $i + \frac{1}{2}$. Then the same relationship can be used for both $\bar{\sigma}^{(1)}_{i+1/2}$ and $\bar{\sigma}^{(2)}_{i+1/2}$

$$\bar{\sigma}^{(k)}_i = \frac{1}{\zeta_2}\int_{x_{i+1/2}-\zeta_2}^{x_{i+1/2}} \sigma^{(k)}_i(x)\,\mathrm{d}x, \quad k = 1, 2 \tag{2.23}$$

If matrix **K** is assumed to be constant over the integration interval, substituting Equation (2.22) into Equation (2.23) gives

$$\phi_{i+1/2,\mathrm{L}} = \frac{1}{\zeta_2} \int_{x_{i+1/2}-\zeta_2}^{x_{i+1/2}} \phi_i(x)\,\mathrm{d}x \tag{2.24}$$

A similar reasoning gives the formula for the right state of the Riemann problem

$$\phi_{i+1/2,\mathrm{R}} = \frac{1}{\zeta_1} \int_{x_{i+1/2}-\zeta_1}^{x_{i+1/2}} \phi_{i+1}(x)\,\mathrm{d}x \tag{2.25}$$

Therefore, in the subcritical case, the left and right states of the Riemann problem can be obtained by simply averaging the reconstructed profile over the domain of dependence of the characteristics.

2.4. Riemann solver

The solution of the Riemann problem consists of a zone of constant state, separated from the left and right states by either shock or rarefaction waves. When the flow is subcritical, the interface between two computational cells will always be located in the intermediate zone of constant state. It is then sufficient to compute this intermediate state to compute the fluxes $F_{i+1/2}$. The Riemann solver used here is an approximate-state solver, i.e. the intermediate state is computed by making an *a priori* assumption on the nature of the rightward and the leftward waves. This classical approach was used by Colella [10] and Dukowicz [11], who made the assumption of two shock waves. A non-iterative solver based on the assumption of two rarefaction waves was devised by the author [4] for constant wave speeds and later adapted to variable speeds. An iterative solver was also presented in the same publication for variable wave speeds [4]. Although iterative, the latter solver produces very accurate results even if a few iterations are performed. Numerical experiments showed indeed that two iterations were sufficient to achieve convergence. Its principle is as follows.

The expression for the kth generalized Riemann invariant [12] can be written as

$$\frac{\mathrm{d}\mu}{\kappa_{k,1}} = \frac{\mathrm{d}q}{\kappa_{k,2}} \text{ across } \mathrm{d}x/\mathrm{d}t = \lambda_k \tag{2.26}$$

where $\kappa_{k,j}$ is the component on the k-th row and j-th column of matrix **K**. As following the first characteristic is equivalent to crossing the second one (and conversely, following the second characteristic is equivalent to crossing the first one), it is easy to check that Equation (2.26) can be rewritten as

$$\lambda_2\,\mathrm{d}\mu - \mathrm{d}q = 0 \text{ along } \mathrm{d}x/\mathrm{d}t = \lambda_1 \tag{2.27a}$$

$$\lambda_1 \, \mathrm{d}\mu - \mathrm{d}q = 0 \text{ along } \mathrm{d}x/\mathrm{d}t = \lambda_2 \tag{2.27b}$$

the two differential relationships ($k = 1$ and $k = 2$) can be approximated according to the trapezium rule with the following expressions

$$q_{i+1/2} - q_{\mathrm{L}} = \frac{1}{2}(u_{i+1/2} - c_{i+1/2} + u_{\mathrm{L}} - c_{\mathrm{L}})(\mu_{i+1/2} - \mu_{\mathrm{L}}) \tag{2.28a}$$

$$q_{i+1/2} - q_{\mathrm{R}} = \frac{1}{2}(u_{i+1/2} + c_{i+1/2} + u_{\mathrm{R}} + c_{\mathrm{R}})(\mu_{i+1/2} - \mu_{\mathrm{R}}) \tag{2.28b}$$

Since $u_{i+1/2} = q_{i+1/2}/\mu_{i+1/2}$ and $c_{i+1/2}$ is a function of $\mu_{i+1/2}$ only. The non-linear system above can be solved using iterative techniques. In practice, between five and ten iterations are needed to achieve convergence of the solver with a precision of 10^{-5} Pa on the pressure and 10^{-7} kg s^{-1} on the mass discharge. However, two iterations only allow convergence with a precision of 0.1 Pa and 10^{-3} kg s^{-1}, which is seen as sufficient for most applications. Note that other types of Riemann solvers, based in particular on Roe's formulation [13], have been used for two-phase problems [14,15].

3. BOUNDARY CONDITIONS

3.1. Algorithm overview

The DPM reconstruction technique uses cells $i-1$, i and $i+1$ to reconstruct the profile in cell i. Consequently the value $\phi_{1,\mathrm{L}}$ cannot be computed directly at the left boundary, because there is no cell to the left of cell 1. The problem is the same at the right boundary for the state $\phi_{N,\mathrm{R}}$, where N is the number of cells in the computational domain. Additional information must then be supplied so that the reconstruction in the first and last cells is possible. Another problem associated with schemes for advection that use one or more downstream cells is that computational results are sensitive to downstream values, even for the scalar advection equation, whereas the analytical solution is sensitive to upstream values only. Here an algorithm is proposed to overcome these two problems. This algorithm is derived from an earlier work conducted by the author on 2×2 systems of linear advection equations [5]. Any attempt to simplify this algorithm and drop part of it was found to reduce considerably the quality of the computational results.

The basic idea of the present algorithm is to add two virtual cells at both ends of the pipe (see Figure 3) so that (i) at least one additional cell is provided for the reconstruction in the cells at both ends of the pipe, and (ii) the outgoing information (i.e. the eigenvectors) is evacuated from the domain without bringing any disturbance to the inner cells. The modified number N^* of cells is equal to $N+4$. The part of the model that represents the real pipe starts at cell 3 and ends at cell N^*-2.

The overall algorithm (including solution computation in the inner cells) comprises three steps:

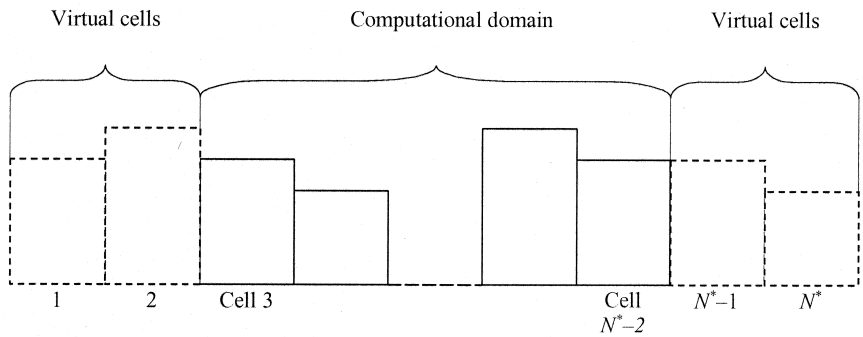

Figure 3. Handling boundary conditions by adding virtual cells at both ends of the computational domain.

(a) determination of the value of the variable ϕ at the boundaries,
(b) determination of the average quantities Φ in the virtual cells,
(c) reconstruction in all cells and computation of fluxes at cell interfaces, including the virtual cells, via the solution of a Riemann problem.

3.2. *Determination of boundary values* ϕ

For the sake of clarity, consider the left-hand boundary only, knowing that the algorithm is exactly the same for the right-hand boundary. At the left-hand boundary, conservation of the first eigenvector can be stated

$$q_{5/2} - q_{5/2,\mathrm{R}} = \frac{1}{2}(u_{5/2} + c_{5/2} + u_{5/2,\mathrm{R}} + c_{5/2,\mathrm{R}})(\mu_{5/2} - \mu_{5/2,\mathrm{R}}) \tag{3.1}$$

where $q_{5/2}$ and $\mu_{5/2}$ are the mass discharge and mass per unit length at the left-hand boundary (interface 5/2) and $q_{5/2,\mathrm{L}}$ and $\mu_{5/2,\mathrm{L}}$ are the averages of the reconstructed profiles over the domain of dependence of the first characteristic passing at 5/2. Note that a first reconstruction has to be performed in cell 3 prior to the averaging.

Another relationship is available from the boundary condition at interface 5/2

$$f_{5/2}(\mu_{5/2}, q_{5/2}) = 0 \tag{3.2}$$

The non-linear system of Equations (3.1) and (3.2) is solved iteratively using any classical technique such as the Newton–Raphson algorithm. This can be easily generalized to a junction

between l pipes. Then, there are l relationships of the form (3.1) and one relationship stating mass conservation (i.e. the sum of all mass discharges at interface 5/2 is equal to 0). The unknowns are the l discharges for each pipe and the mass per unit length at the interface, which is the same for all pipes (because the pressure is the same). Therefore, the solution is unique.

3.3. Computation of virtual cell averages Φ

Consider the left-hand boundary once again. The previous work mentioned above [5] showed that the most efficient way of handling boundary conditions via virtual cells consists of leaving the outgoing eigenvector (here $\sigma^{(1)}$) unchanged and modifying the impinging one (here $\sigma^{(2)}$) so that its reconstruction in cell 2 is in agreement with the value at interface $\frac{1}{2}$, in other words

$$\sigma^{(2)}_{2,\mathrm{L}} = \sigma^{(2)}_{5/2} \tag{3.3}$$

The simplest way to do so is to set the values of $\sigma^{(2)}$ in cells 1 and 2 according to

$$\sigma^{(2)}_1 = \sigma^{(2)}_2 = \sigma^{(2)}_{5/2} \tag{3.4}$$

Assume that a previous computation has produced the values μ_1, q_1, μ_2, q_2, of the mass per unit length and the mass discharge in cells 1 and 2 respectively. First compute the vector σ in cells 1 and 2

$$\sigma_j = \mathbf{K}^{-1}\begin{bmatrix}\mu_j\\ q_j\end{bmatrix} = \frac{1}{2c}\begin{bmatrix}\lambda_2 & -1\\ -\lambda_1 & 1\end{bmatrix}\begin{bmatrix}\mu_j\\ q_j\end{bmatrix} = \frac{1}{2c}\begin{bmatrix}\lambda_2\mu_j - q_j\\ -\lambda_1\mu_j + q_j\end{bmatrix}, \quad j = 1, 2, 5/2 \tag{3.5}$$

where c, λ_1 and λ_2 are computed at interface 5/2. The index 5/2 is dropped for the sake of clarity. Applying the rule given by Equation (3.4) yields the updated representation σ^*_j of ϕ in the base of eigenvectors in cells $j = 1, 2$

$$\sigma^*_j = \frac{1}{2c}\begin{bmatrix}\lambda_2\mu_j - q_j\\ -\lambda_1\mu_{5/2} + q_{5/2}\end{bmatrix} \quad j = 1, 2 \tag{3.6}$$

Returning to the modified primary variable Φ^* by multiplying σ^*_j by matrix $\mathbf{K}$

$$\Phi^*_j = \frac{1}{2c}\begin{bmatrix}\lambda_2\mu_j - \lambda_1\mu_{5/2} - q_j + q_{5/2}\\ \lambda_1\lambda_2(\mu_j - \mu_{5/2}) - \lambda_1 q_j + \lambda_2 q_{5/2}\end{bmatrix} \quad j = 1, 2 \tag{3.7}$$

Note that the same matrix $\mathbf{K}$ is used for the left boundary and for cells 1 and 2. Although not strictly rigorous, this provides the economy of an iterative procedure for the determination of $\mathbf{K}$ in cells 1 and 2. The quality of the results was seen not to be affected significantly by the present simplification. A similar reasoning for the right-hand boundary gives

$$\Phi_j^* = \frac{1}{2c}\begin{bmatrix} \lambda_2\mu_{N^*-5/2} - \lambda_1\mu_j - q_{N^*-5/2} + q_j \\ \lambda_1\lambda_2(\mu_{N^*-5/2} - \mu_j) - \lambda_1 q_{N^*-5/2} + \lambda_2 q_j \end{bmatrix} \quad j = N^*-1, N^* \tag{3.8}$$

where λ_1 and λ_2 are computed at interface $N^* - 5/2$.

3.4. Reconstruction and flux computation

The reconstruction is performed in all cells, including the virtual ones. The right and left states in the virtual cells are set equal to the average cell value so as to respect the condition given by Equation (3.4). The reconstruction in the inner cells is performed as explained in Section 2.1.

The fluxes through interfaces 3/2 to $N^* - 1/2$ are computed by solving the Riemann problem defined according to Section 2.3, except at interfaces 5/2 and $N^* - 3/2$ (which represent the extremities of the pipe) where the solution of the system of Equations (3.1) and (3.2) is used for flux computation.

The mass balance is then performed on cells 2 to $N^* - 1$ according to Equation (2.1). Finally, we update the outgoing eigenvector in cell 1 (resp. N^*) by setting it equal to its value in cell 2 (resp. $N^* - 1$). To do so, we set Φ_1 equal to Φ_2 and Φ_{N^*} equal to Φ_{N^*-1}. Note that it is essential to perform the mass balance on cells 2 and $N^* - 1$ and to update cells 1 and N^*, for this ensures the correct advection of the outgoing eigenvectors through the pipe boundaries. Suppressing one of these two steps was observed to degrade the quality of the results.

3.5. Internal boundary conditions

Internal boundary conditions can be dealt with using the algorithm described above, but more than one pipe (in general m) may be present and joined together. In that case, m equations of the type (3.1) can be written at each pipe end. The law of nodes provides another equation

$$\sum_{l=1}^{m} q_{5/2,l} = 0 \tag{3.9}$$

where $q_{5/2,l}$ is the discharge entering pipe l at the boundary. Moreover the laws for head loss at each pipe extremity allow $m - 1$ independent equations to be written of the type

$$f_m(\mu_{5/2,m}, q_{5/2,m}) = f_{m'}(\mu_{5/2,m'}, q_{5/2,m'}) \text{ for any } (m, m') \tag{3.10}$$

There are therefore $2m$ equations for $2m$ unknowns (the mass per unit length and discharge at each boundary), which means there is a unique solution to the problem. The set of equations (3.10) is in general non-linear and has to be solved iteratively. Once the values $(\mu_{5/2,m}, q_{5/2,m})$ are known at each pipe boundary, the algorithm described in Sections 3.1 to 3.3 can be applied.

4. COMPUTATIONAL EXAMPLE

The performance of the scheme was illustrated by computing the flow that results from the sudden opening of a valve located at the midpoint of a pipe. It is very similar to the shock tube problem

in gas dynamics or to the dambreak problem in shallow water simulations. The pipe and fluid parameters are presented in Table I. Table II indicates the initial and boundary conditions. The pipe has a length of 3000 m, the valve is located at $x = 1500$ m. The fluid is initially at rest. The pressure is 5×10^5 Pa left of the pipe and 10^5 Pa on its right-hand side. Both ends of the pipe are closed and allow no flow. The opening of the valve results in the appearance of a shock wave and of a rarefaction fan travelling in opposite directions. Both waves are reflected at the pipe extremities and their nature changes from shock to rarefaction every second reflection. The numerical solution was compared with an approximate analytical one derived for times smaller than 2 s, i.e. before the rarefaction wave reaches the pipe extremity. The flow was computed over 80 s using cell sizes ranging from 10 to 100 m. In order to provide a basis for comparison, the time step for each of the simulations was chosen such that the maximum value of the Courant number was equal to unity. Figure 4 shows the profiles obtained using the Godunov and DPM schemes at time $t = 2$ s. This corresponds to the time at which the rarefaction wave heading to the left reaches the pipe extremity. At further times, owing to the no-flow condition, the pressure at the left-hand boundary drops extremely fast. For this reason, in addition to testing the ability of the scheme to take into account shock and rarefaction waves, this test indicates very clearly whether computed waves propagate at the correct speed. Figure 4 shows that both the original Godunov and the DPM schemes introduce artificial front smearing for a cell size $\Delta x = 100$ m. Still, it will be observed that the width of the shock computed with the DPM scheme is only two thirds of that computed by the Godunov scheme. Decreasing the cell size down to 10 m did not allow the head of the rarefaction wave to be located properly by the Godunov scheme, whereas the

Table I. Physical parameters for test case 1.

Parameter	Symbol and unit	Value
Pipe length	L (m)	3000
Nominal cross-sectional area	A_0 (m^2)	0.29
Nominal celerity	c_0 (m s^{-1})	981.4
Nominal density	ρ_0 (kg m^{-3})	992
Coefficient in the perfect gas equation	α	1
Reference mass per unit length	μ_0 (kg m^{-1})	289.9
Reference void fraction	$\eta_{g,0}$	2×10^{-3}
Reference pressure	p_0 (Pa)	101 325

Table II. Initial and boundary conditions for test case 1.

Parameter	Symbol and unit	Value
Initial mass discharge	q_i (kg s^{-1})	0
Initial pressure	P_i (Pa)	5×10^5 for $x < 1500$ m, 10^5 for $x \geq 1500$ m
Discharge at the left end of the pipe	q_{LE} (Pa)	0
Discharge at the right end of the pipe	q_{RE} (Pa)	0

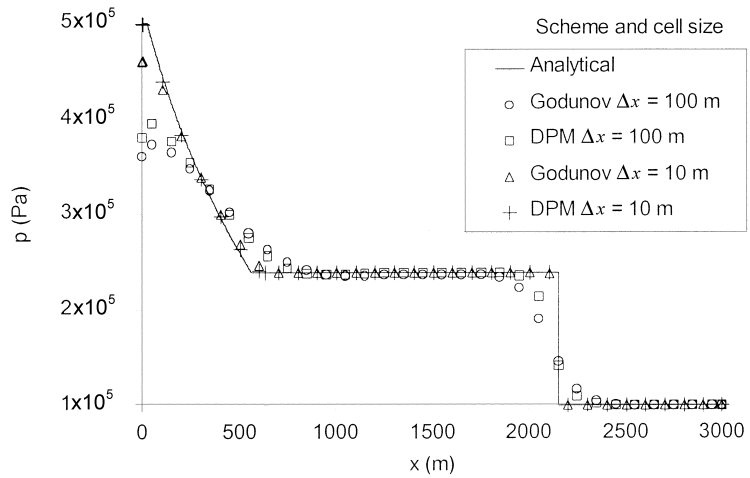

Figure 4. Test case 1: computed pressure profiles by the original Godunov and DPM schemes at time $t = 2$ s.

DPM proved to be able to track it accurately. For the readability of Figure 4, the profiles for $\Delta x = 10$ m were drawn using every tenth point. Figure 5 shows the pressure history computed by the Godunov and DPM schemes at the middle of the pipe (that is the location of the initial pressure discontinuity) for various cell sizes. It can be seen that the amplitude of the computed oscillations is larger when the DPM is used than with the Godunov scheme. This was confirmed by experiments carried out using various values of Δx. These results are not displayed for the sake of readability of the figure. Table III and Figure 6 show the average amplitude of the first ten oscillations obtained for various cell sizes. The amplitudes were normalized with the amplitude given by the DPM on a cell size of 10 m. It can be seen that it is sufficient to use the DPM scheme with a cell size of 25 m to obtain a satisfactory convergence of the amplitude, whereas it is necessary to decrease Δx to 10 m when the Godunov scheme is used. The improvement brought by the DPM over the Godunov scheme is confirmed by a number of test cases involving a variety of initial and boundary conditions (more test cases and comparisons with the original Godunov scheme can be found in [16]). From these cases, it was concluded that the DPM needs in general four to five times fewer cells than the first-order Godunov scheme to achieve the same accuracy.

5. CONCLUSIONS

The application of higher-order Godunov schemes to the computation of two-phase pipe transients has been investigated. The efficiency of Godunov-type algorithms can be increased

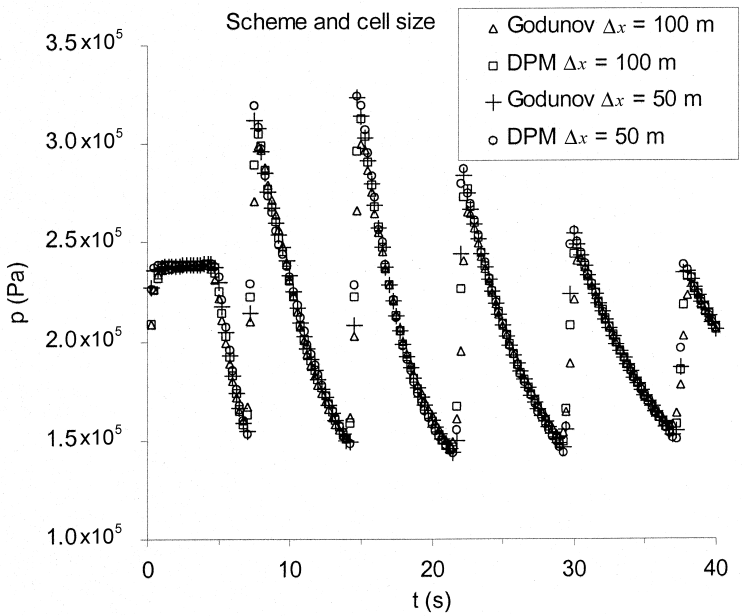

Figure 5. Pressure histories at the middle of the pipe for various schemes and cell sizes.

Table III. Average amplitude for various cell sizes.

Average amplitudes normalized with DPM $\Delta x = 10$ m (percentages)							
Godunov $\Delta x = 100$ m	DPM $\Delta x = 100$ m	Godunov $\Delta x = 50$ m	DPM $\Delta x = 50$ m	Godunov $\Delta x = 25$ m	DPM $\Delta x = 25$ m	Godunov $\Delta x = 10$ m	DPM $\Delta x = 10$ m
79.7	86.5	92.7	96.1	98.1	100.0	99.5	100

Values are given as percentages. The values obtained with the DPM for $\Delta x = 10$ m are taken as the reference (100 per cent).

by improving the reconstruction technique. The DPM, detailed in the present contribution, allows fronts to be located more accurately than the original Godunov technique. The Riemann problem can be solved using an iterative, approximate-state solver based on the assumption of two rarefaction waves. Performing a few iterations only (typically two or three) allows the Riemann problem to be solved with a good accuracy. The treatment of boundary conditions turns out to be another key factor in the scheme efficiency. The best performances are achieved by implementing two virtual cells at each end of the computational domain. The outgoing wave component is advected beyond the boundary into the virtual cells in order to ensure independence of the solution from the downstream boundary condition. The impinging wave component is modified in the virtual cells so that its reconstruction yields the value that

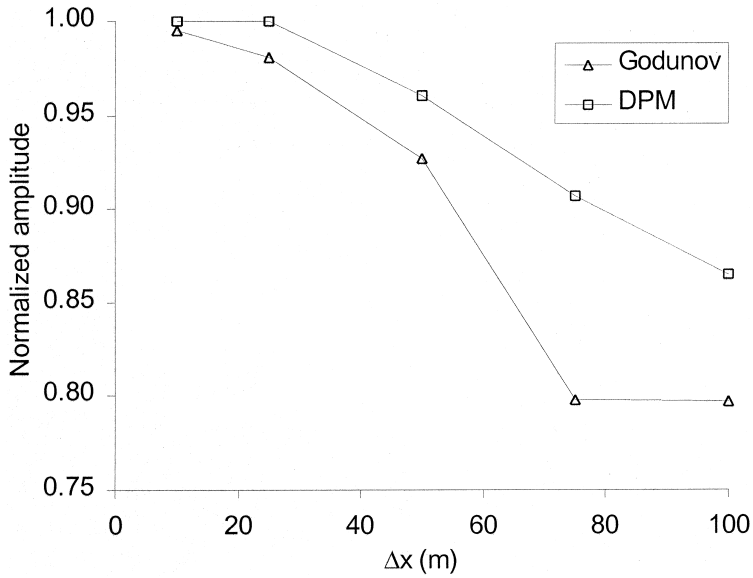

Figure 6. Average amplitude ratio obtained using the Godunov and DPM scheme for various cell sizes.

is prescribed at the boundary. The performances of the DPM scheme are illustrated by a case that is representative of classical pipe network operations. A comparison between the results given by the first-order Godunov scheme and the DPM shows that the latter needs four to five times fewer cells than the former for a comparable quality of the computational results.

ACKNOWLEDGMENTS

The author would like to thank Professors J.A. Cunge and M.J. Hall from IHE for their review, comments and suggestions on this paper.

APPENDIX A. EIGENVALUES AND EIGENVECTORS

The equations to be solved are

$$\frac{\partial \phi}{\partial t} + \frac{\partial F}{\partial x} = 0 \tag{1.1a}$$

$$\phi = \begin{bmatrix} \mu \\ q \end{bmatrix}, \qquad F = \begin{bmatrix} q \\ Ap + q^2/\mu \end{bmatrix} \tag{1.1b}$$

$$\frac{\mathrm{d}}{\mathrm{d}\mu}(Ap) = c^2 = \frac{c_w^2}{1 + \theta/p^{1+1/\alpha}} \tag{1.1c}$$

$$\theta = \eta_0 \rho_0 c_w^2 p_0^{1/\alpha} \tag{1.1d}$$

$$p\eta^{\alpha} = p_0 \eta_0^{\alpha} \tag{1.1e}$$

$$\rho_g \eta = \rho_{g,0} \eta_0 \tag{1.1f}$$

Equation (1.1a) can also be rewritten under the non-conservative advection form

$$\frac{\partial \phi}{\partial t} + \mathbf{M} \frac{\partial \phi}{\partial x} = 0 \tag{A.1a}$$

$$\mathbf{M} = \begin{bmatrix} 0 & 1 \\ \dfrac{\partial}{\partial \mu}(Ap + q^2/\mu) & \dfrac{\partial}{\partial q}(Ap + q^2/\mu) \end{bmatrix} \tag{A.1b}$$

Substituting Equation (1.1c) into Equation (A.1b) and noticing that the velocity u is given by $u = q/\mu$, after some straightforward algebra, yields

$$\mathbf{M} = \begin{bmatrix} 0 & 1 \\ c^2 - u^2 & 2u \end{bmatrix} \tag{A.2}$$

The two eigenvalues λ_k, $k = 1, 2$ of $\mathbf{M}$ satisfy the following relationship

$$\mathrm{Det}\begin{bmatrix} -\lambda_k & 1 \\ c^2 - u^2 & 2u - \lambda_k \end{bmatrix} = 0 \tag{A.3}$$

which yields

$$\lambda_k = u + (-1)^k c, \quad k = 1, 2 \tag{A.4}$$

It is easy to check that the eigenvector $e^{(k)}$ associated with the eigenvalue λ_k, $k = 1, 2$ is given by

$$e^{(k)} = \begin{bmatrix} 1 \\ \lambda_k \end{bmatrix} \tag{A.5}$$

The matrix $\mathbf{K}$ formed by the base of the eigenvectors is therefore the following

$$\mathbf{K} = \begin{bmatrix} 1 & 1 \\ \lambda_1 & \lambda_2 \end{bmatrix} \tag{A.6}$$

REFERENCES

1. Wylie EB, Streeter VL. *Fluid Transients in Systems*. Prentice-Hall: Engelwood Cliffs, NJ, 1993.
2. Wylie EB. Simulation of vaporous and gaseous cavitation. *Journal of Fluids in Engineering*, *ASME* 1984; **106**: 307–311.
3. Zielke W, Perko HD, Keller A. Gas release in transients pipe flow. In *6th International Conferences on Pressure Surges*, *BHRA*, Cambridge, UK. BHR Group: Cambridge, 1989; 3–13.
4. Guinot V. Numerical simulation of two-phase flow in pipes using Godunov method. *International Journal for Numerical Methods in Engineering* 2001; **50**: 1169–1189.
5. Guinot V. Boundary condition treatment in 2×2 systems of propagation equations. *International Journal for Numerical Methods in Engineering* 1988; **42**: 647–666.
6. Godunov SK. A difference method for numerical calculation of discontinuous equations of hydrodynamics (in Russian). *Matematicheski Sbornik* 1959; **47**: 271–300.
7. van Leer B. Toward the ultimate conservative difference scheme, V: a second-order sequel to Godunov's method. *Journal of Computational Physics* 1979; **32**: 101–136.
8. Ben-Artzi M, Falcovitz J. A second-order Godunov-type scheme for compressible fluid dynamics. *Journal of Computational Physics* 1984; **55**: 1–32.
9. Colella P, Woodward PR. The piecewise parabolic method (PPM) for gas-dynamical simulations. *Journal of Computational Physics* 1984; **54**: 174–201.
10. Colella P. Glimm's method for gas dynamics. *SIAM Journal of Scientific and Statistical Computing* 1982; **3**(1): 76–110.
11. Dukowicz J. A general, non-iterative Riemann solver for Godunov's method. *Journal of Computational Physics* 1985; **61**: 119–137.
12. Jeffrey A, Taniuti T. *Non-linear Wave Propagation*. Academic Press: New York, 1964.
13. Roe PL. Approximate Riemann solvers, Parameter vectors and difference schemes. *Journal of Computational Physics* 1981; **43**: 357–372.
14. Toumi I. A weak formulation of Roe's approximate Riemann solver. *Journal of Computational Physics* 1992; **102**: 360–373.
15. Toumi I, Kumbaro A. An approximate linearized Riemann solver for a two-fluid model. *Journal of Computational Physics* 1996; **124**: 286–300.
16. Guinot V. Modelling two-phase flow in pipes using Godunov-type algorithms. IHE Research Report HH424/99/1. HTML version: http://www.ihe.nl/hi/guinot/vgt05/Report01.htm, 1999.

